Origin of Convectively Coupled Kelvin Waves over South America

BRANT LIEBMANN,* GEORGE N. KILADIS,+ LEILA M. V. CARVALHO,# CHARLES JONES,@ CAROLINA S. VERA,& ILEANA BLADÉ,** AND DAVE ALLURED*

* *NOAA/Earth System Research Laboratory, and CIRES Climate Diagnostics Center, Boulder, Colorado*
+ *Physical Sciences Division, NOAA/Earth System Research Laboratory, Boulder, Colorado*
# *Department of Atmospheric Sciences, Institute of Astronomy, Geophysics and Atmospheric Sciences, University of São Paulo, São Paulo, Brazil*
@ *Institute for Computational Earth System Science, University of California, Santa Barbara, Santa Barbara, California*
& *Department of Atmospheric and Ocean Sciences, CIMA/UBA-CONICET, Buenos Aires, Argentina*
** *Departament d'Astronomia i Meteorologia, Universitat de Barcelona, Barcelona, Spain*

(Manuscript received 26 November 2007, in final form 23 June 2008)

ABSTRACT

Convectively coupled Kelvin waves over the South American continent are examined through the use of temporal and spatial filtering of reanalysis, satellite, and gridded rainfall data. They are most prominent from November to April, the season analyzed herein. The following two types of events are isolated: those that result from preexisting Kelvin waves over the eastern Pacific Ocean propagating into the continent, and those that apparently originate over Amazonia, forced by disturbances propagating equatorward from central and southern South America.

The events with precursors in the Pacific are mainly upper-level disturbances, with almost no signal at the surface. Those events with precursors over South America, on the other hand, originate as upper-level synoptic wave trains that pass over the continent and resemble the ''cold surges'' documented by Garreaud and Wallace. As the wave train propagates over the Andes, it induces a southerly low-level wind that advects cold air to the north. Precipitation associated with a cold front reaches the equator a few days later and subsequently propagates eastward with the characteristics of a Kelvin wave. The structures of those waves originating over the Pacific are quite similar to those originating over South America as they propagate to eastern South America and into the Atlantic.

South America Kelvin waves that originate over neither the Pacific nor the midlatitudes of South America can also be identified. In a composite sense, these form over the eastern slope of the Andes Mountains, close to the equator. There are also cases of cold surges that reach the equator yet do not form Kelvin waves.

The interannual variability of the Pacific-originating events is related to sea surface temperatures in the central–eastern Pacific Ocean. When equatorial oceanic conditions are warm, there tends to be an increase in the number of disturbances that reach South America from the Pacific.

1. Introduction

Convectively coupled Kelvin waves are a predominant feature of the tropical circulation (e.g., Takayabu and Murakami 1991; Takayabu 1994; Dunkerton and Crum 1995; Wheeler and Kiladis 1999; Wheeler et al. 2000; Roundy 2008). Kelvin waves occur over the entire equatorial band, but are particularly prominent over the equatorial Pacific. They propagate eastward at between 10 and 20 m s^{-1}, and their horizontal structure broadly resembles that expected from shallow-water theory (Straub and Kiladis 2002, 2003b). Strong modulation of deep convection occurs within Kelvin waves, and their convective envelopes are generally composed of a variety of mesoscale convective elements propagating both eastward and westward (Straub and Kiladis 2002).

The globally averaged variance of outgoing longwave radiation (OLR), filtered to retain only Kelvin wave activity (Wheeler and Kiladis 1999), is largest in the northern spring, which is also the season of strongest activity over South America. This maximum OLR variance over South America is centered slightly north of the equator and is an extension of the global maximum

Corresponding author address: Brant Liebmann, Cooperative Institute for Research in Environmental Sciences Climate Diagnostics Center, Campus Box 216, Boulder, CO 80309-0216.
E-mail: Brant.Liebmann@noaa.gov

DOI: 10.1175/2008JCLI2340.1

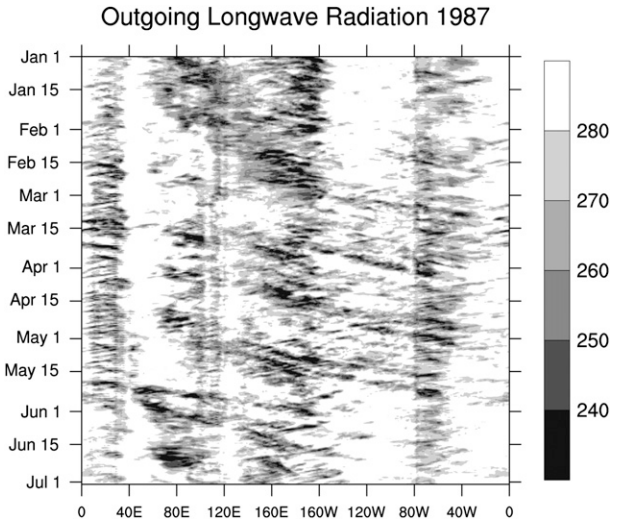

FIG. 1. Hovmöller diagram of CLAUS T_b (K) averaged from 5°N to 5°S for dates indicated in 1987. Resolution of plot is twice daily and 0.5° lon.

located in the central Pacific during that season (Straub and Kiladis 2002; Roundy and Frank 2004).

Kelvin waves propagating eastward from South America may play an important role in modulating convective activity downstream. For instance, Wang and Fu (2007) recently showed that variations of the Atlantic intertropical convergence zone (ITCZ) in the northern spring are influenced by Kelvin wave activity propagating from South America. These Kelvin waves have also been shown to influence the West African monsoon (Mounier et al. 2007) and convective precipitation in eastern Africa (Mekonnen et al. 2008) during the northern summer, as well as mesoscale organization over central Africa during northern spring (Nguyen and Duvel 2008). All of these studies noted that some of the Kelvin waves affecting Africa appeared to originate over the central and eastern Pacific.

Figure 1 shows a Hovmöller diagram of high-resolution OLR averaged about the equator for January–July 1987, an active period for the Kelvin waves over the eastern Pacific. The west coast of South America along the Andes Mountains stands out as a discontinuity in this diagram at about 80°W, because the mean brightness temperature T_b is lower over the continent than the adjacent ocean. In Fig. 1 many disturbances propagating eastward from the central–eastern Pacific amplify dramatically as they reach the continent. Many of these Kelvin-like waves moving from South America into the Atlantic seem to originate in the Pacific and pass over South America, unimpeded by the Andes barrier, whose elevation near the equator averages around 3000 m. Some of these disturbances, however, appear to originate over the continent (e.g., those in January). The purpose of the work presented here is to better understand the origins of the eastward-propagating disturbances that move from South America into the Atlantic. We will show that, indeed, a substantial fraction of the Kelvin waves observed over South America appear to be triggered by cold-air outbreaks or ''cold surges'' reminiscent of the events documented by Garreaud and Wallace (1998) and Garreaud (2000).

After describing the data and how they are filtered in section 2, the results are presented in section 3. This section includes a description of different ways that Kelvin waves come to be over South America, and an estimate of their contribution to summertime rainfall amounts. The results are summarized in section 4.

2. Data

The period chosen for the analysis is the extended Southern Hemisphere winter season (November–May) from 1979/80 to 2005/06. The National Oceanic and Atmospheric Administration daily OLR begins in 1979 (after a long gap in 1978). Missing values have been filled in by linear interpolation (Liebmann and Smith 1996). Figure 1, however, was made using high-resolution Cloud Archive User Service (CLAUS) satellite brightness temperature data. This dataset was assembled by merging geostationary and polar-orbiting satellite irradiance onto a global grid with 0.5° and 8-times daily resolution (Hodges et al. 2000). Daily wind fields at 2.5° spatial resolution were obtained from the National Centers for Environmental Prediction Reanalysis I (Kalnay et al. 1996). Streamfunction is calculated from the wind components using spherical harmonic routines. Rainfall data are from the South American dataset described by Liebmann and Allured (2005), also at daily 2.5° resolution. Missing precipitation data points were not filled. The rainfall data over the Amazon is of a sufficient density to capture the scales of interest here (e.g., Liebmann et al. 1998).

Two filters were used in the analysis. One retains only the Kelvin components by spatial and temporal filtering, as specified by Straub and Kiladis (2002, see their Fig. 1). This filter retains only eastward-propagating OLR signals within the space–time region of the spectral peak associated with Kelvin waves. At its low-frequency cutoff (near an 18-day period) it is centered on zonal wavenumbers 1–3, extending out to wavenumbers 8–15 at its high-frequency end at around a 1.75-day period. At 0°, 60°W, one of the key locations for the present analysis, 15% of the total November–May daily OLR variance is captured by the Kelvin-filtered time series. The other filter is a high pass with a cutoff frequency of

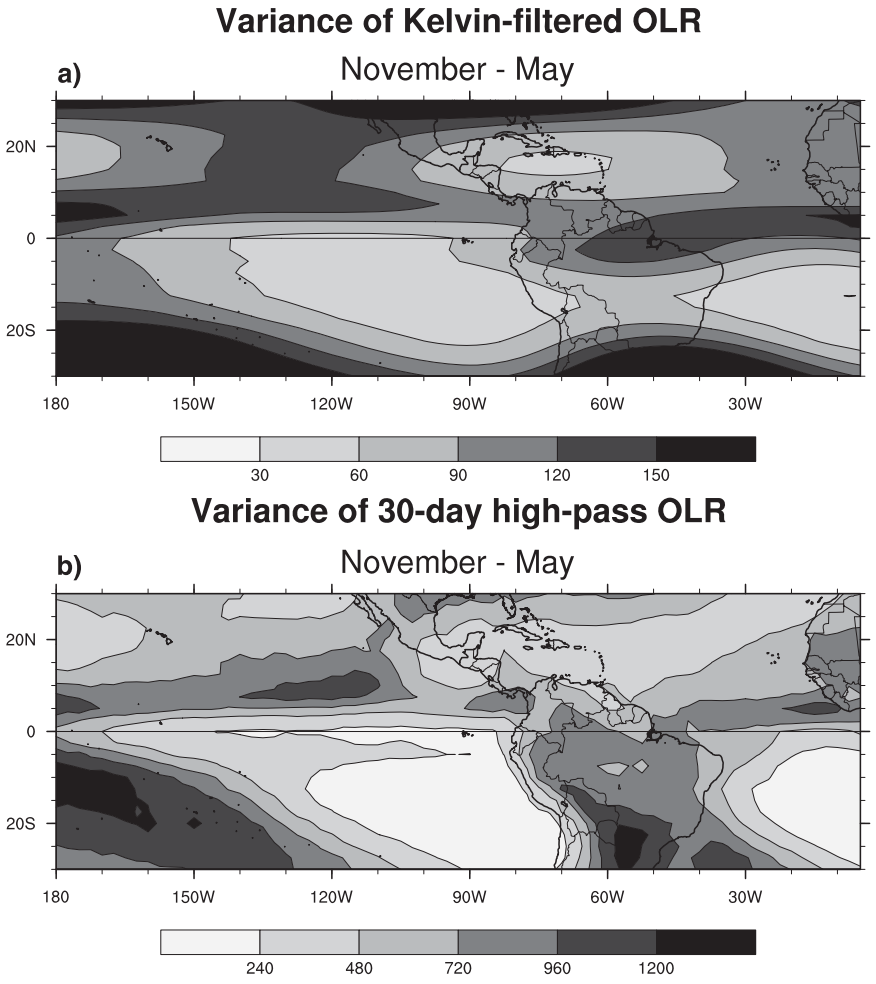

FIG. 2. Variance ($W^2\ m^{-4}$) of (a) Kelvin-filtered and (b) 30-day high-pass-filtered OLR anomaly for November–May 1979/80–2005/06 period. Note shading intervals of (b) are 8 × (a).

30 days. A 119-weight Lanczos filter (Duchon 1979) was used to obtain a sharp spectral cutoff. At 0°, 60°W, 73% of the total November–May daily OLR variance is explained by the high-pass 30-day-filtered time series. Whenever a gap is found at time t at a particular grid point in the precipitation dataset, the filtered value for days $t - 59$ to $t + 59$ is set to missing.

3. Results

a. Seasonal cycle

Figure 2a shows the climatological variance of daily Kelvin-filtered OLR computed for November–May, which is the period of interest for this study. These months were chosen after examining the seasonal analysis of Kelvin wave activity presented by Roundy and Frank (2004), and from variance calculations for individual months (not shown), all of which show a relative maximum over equatorial South America from November to May. This maximum is seen in Fig. 2a, extending into the Atlantic, although it is slightly displaced north of the equator along the climatological position of the ITCZ. Over the eastern Pacific, the maximum Kelvin wave variance is located between 5°– and 10°N, diminishing as it approaches South America. This off-equatorial OLR maximum is not entirely unexpected. In a case study of a convective disturbance propagating eastward over the eastern Pacific, Straub and Kiladis (2002) showed that while the wind field was symmetric about the equator and consistent with the theoretical structure of a Kelvin wave, the associated heating field (as indicated by OLR) was centered north of the equator, collocated with warm sea surface temperatures (SSTs) and the ITCZ.

For comparison with Fig. 2a, high-pass OLR variance with a 30-day cutoff (therefore including the Kelvin

wave frequencies) is presented in Fig. 2b. While the two maps are qualitatively similar near the equator, the shading interval is 8 times larger in Fig. 2b, illustrating the relatively small amount of total variance contained in the Kelvin wave band.

To further illustrate the seasonality of the Kelvin band activity over South America, the standard deviation of Kelvin-filtered OLR at 0°, 60°W was calculated for the entire record. The percent of negative anomalies larger than 1.5 standard deviations is then plotted as a function of calendar month in Fig. 3. Few strong negative anomalies occur from June to September, even though the strongest cold surges in South America occur during winter (e.g., Parmenter 1976; Marengo et al. 1997; Garreaud 2001). This is presumably because the winter dry season is characterized by strong convective inhibition energy over the Amazon (Fu et al. 1999), so that dynamically forced upward motion would not be manifested in the OLR field. The number of low OLR anomalies increases during October, but the variance plot of that month indicates a minimum over the equatorial Amazon (not shown), so October was not included in the subsequent analysis.

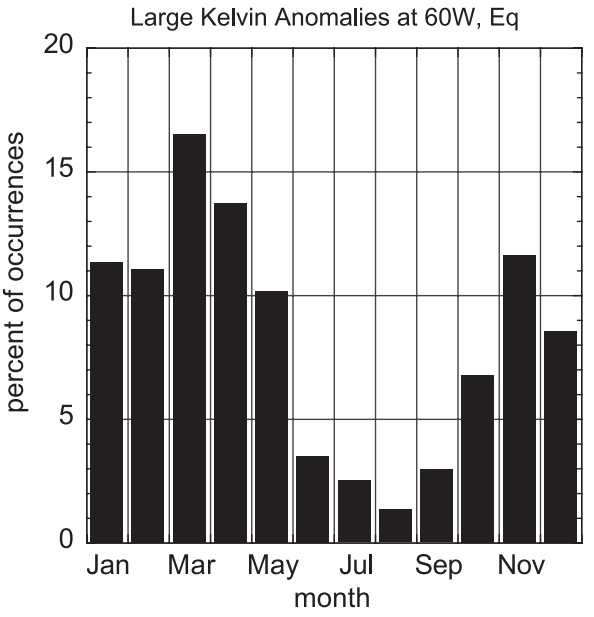

FIG. 3. Climatological percent of occurrences during each month of all Kelvin-filtered OLR anomalies larger than 1.5 std devs below mean at 0°, 60°W.

b. Time evolution

To illustrate the evolution of Kelvin waves propagating across equatorial South America, Fig. 4 shows the total unfiltered OLR and 200-mb wind and streamfunction regressed upon Kelvin-filtered OLR at 0°, 60°W for various leads and lags. The fields represent anomalies associated with a Kelvin-filtered OLR anomaly of -25 W m^{-2}, a typical value for an individual event. When OLR and streamfunction lead the base-point OLR by 3 days (Fig. 4a), anomalously high OLR occurs at the base point, indicating suppressed convection. Patches of low OLR are evident in the eastern Pacific, centered slightly north of the equator, consistent with the mean position of the ITCZ and with the maximum in Kelvin variance (Fig. 2). Also evident is a band of low OLR parallel to, but southwest of, the mean position of the South Atlantic convergence zone (SACZ; e.g., Nogués-Paegle and Mo 1997). It is accompanied by a Southern Hemisphere wave train that appears to have originated in the midlatitudes. One day later (Fig. 4b), strongly negative OLR anomalies have developed on the equator over western South America and the suppressed region of equatorial cloudiness has moved eastward, while the midlatitude wave train continues its progression into the Atlantic.

The simultaneous regression (Fig. 4c), as expected, displays a strong convective anomaly over the base point, while the circulation field bears some resemblance to the Kelvin–Rossby wave response to equatorial heating in the presence of easterlies (e.g., Lim and Chang 1983, their Fig. 2c). The cyclonic anomaly in the southeast quadrant relative to the heating appears as an extension of the midlatitude wave train. Two days later (Fig. 4d) the cyclonic anomaly has moved eastward and positive OLR anomalies have developed over western South America.

Figures 4a,b suggest that the strong convection that develops west of the base point on day -2 (and subsequently propagates eastward as a Kelvin wave) occurs as a result of the merging of the OLR anomalies to the west and south on day -3. Alternatively, these OLR anomalies may be independent phenomena, both of which are representative of convection over equatorial South America at different times, which would still appear together in a regression plot. We will present evidence that this is indeed the case by computing composites that are based on Kelvin-filtered OLR at the base point and subject to additional criteria. This procedure will allow us to separate preexisting Kelvin wave events simply propagating from the west from those initiated in situ forced by disturbances originating to the south.

Selecting those days for which Kelvin-filtered OLR is lower than 1.5 standard deviations below the residual mean (-16.9 W m^{-2}) at the base point (0°, 60°W) results in a sample size of 369 days. Note that the threshold is different than that used to determine the climatology shown in Fig. 3 because the present analysis includes

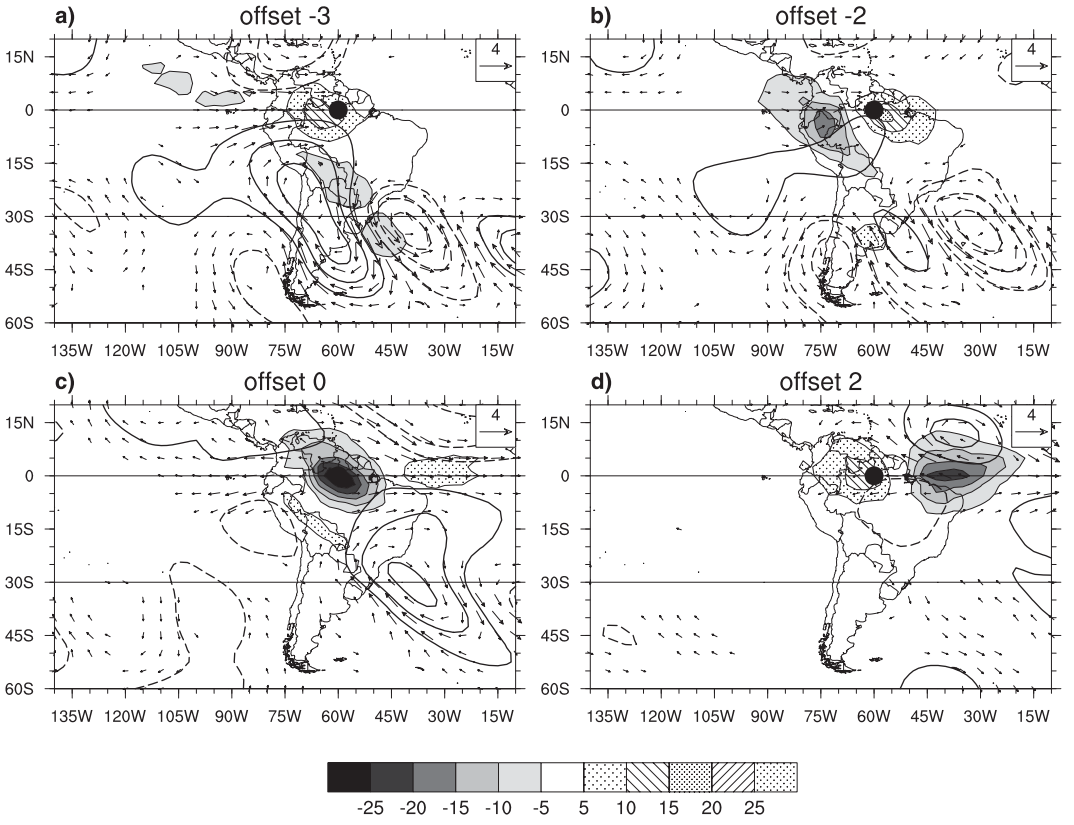

FIG. 4. Daily unfiltered OLR (shaded) and 200-mb wind vectors and streamfunction [contour interval (CI) = 7×10^5 m^2 s^{-1}] regressed onto Kelvin-filtered OLR anomalies of -25 W m^{-2} at 0°, 60°W for (a) fields leading the index by 3 days; (b) fields leading the index by 2 days; (c) fields simultaneous with the index; and (d) fields lagging the index by 2 days. Negative contours dashed and 0 contour omitted. Reference wind vector of 4 m s^{-1} is in upper-right.

only the November–May season. There are 299 individual events, with an ''event'' being defined as a period with OLR staying below the threshold, and day 0 being defined as the day of minimum OLR within an event. Lead and lag composites using all cases are qualitatively similar to the regression in Fig. 4 (not shown).

To separate those events that result from eastward-moving disturbances along the equator from those that are generated by disturbances that propagate to the equator from the south, additional criteria are required for events to be included in a given composite. These additional criteria are chosen based on Fig. 4a, the regression with the fields leading OLR at the base point by 3 days, that is, on the day prior to the merging of the two OLR anomalies. To isolate eastward-propagating Kelvin waves originating in the Pacific, the Kelvin-filtered OLR anomaly at 2.5°N, 95°W must be -16 W m^{-2} on day -3 (i.e., 3 days prior to the peak time of convection at the base point), consistent with an eastward-propagating convective disturbance at a phase speed of ~15 m s^{-1}. The -16 W m^{-2} threshold is approximately the magnitude of the anomaly required to qualify as an event at the base grid point. If there are consecutive dates that qualify, only the date of the sequence with the largest anomaly over South America is included in the composite. This additional criterion yields 53 events for this composite.

To focus on northward-moving disturbances, an additional criterion is that on day -3, the 30-day high-pass-filtered OLR anomaly at 20°S, 60°W must be at least 1.5 standard deviations below the residual mean (-50.6 W m^{-2}). The 30-day high-pass anomalies are used to isolate the precursors to the south because the Kelvin filter emphasizes eastward-propagating disturbances. The additional criterion eliminates all but 48 of the equatorial South America Kelvin wave events. There are four events common to both composites. Recall that because there are missing data in the precipitation field, a precipitation composite may include fewer cases at some grid points.

The choice of locations, thresholds, and lead times by which to separate the equatorial Pacific from the South America events may seem somewhat subjective (as are the location and threshold for the base point), but tests

reveal that the results are quite robust to a wide range of criteria. The lead time was chosen from the regression at day −3 (Fig. 4a) because this is the last day with two distinct OLR anomalies (Fig. 4b). The specific locations within the precursor patterns at day −3 were picked based on the statistical characteristics of Kelvin waves, but experimentation with different nearby locations yields approximately the same results. The precursor thresholds were chosen to yield the approximate same number of dates for both sets of composites. In general, a smaller threshold results in a smoother pattern of a lower amplitude, while a more negative threshold results in a noisier but larger-amplitude pattern. The qualitative structure of the fields, however, remains the same.

There is some seasonality to the events. The frequency of events initiated from the Pacific is slightly below the November–May average in November, drops further in January and December, and increases thereafter. Events associated with disturbances propagating from midlatitude South America are fairly evenly distributed from November to April, with a slight increase in January and February, they but fall off sharply in May.

c. Pacific precursor

Figure 5 shows composites of 30-day high-pass-filtered 200-mb wind, 200-mb streamfunction, and OLR for those events at 0°, 60°W that are preceded by negative Kelvin-filtered OLR anomalies to the west. The most prominent feature at day −4 (Fig. 5a) is a negative OLR anomaly in the eastern Pacific centered slightly north of the equator. This anomaly can be tracked back as originating farther west a few days prior to day −4 (not shown), with no obvious precursor in the wind field. Some Kelvin waves originating in the eastern Pacific are forced by midlatitude Rossby wave trains propagating into the western tropical Pacific from the South Indian Ocean (Straub and Kiladis 2003a). At day −3 (Fig. 5b), the OLR anomaly has moved eastward, and the 200-mb wind field shows some sign of responding to the anomalous heating associated with the OLR anomaly. East of the OLR anomaly, at the longitudes at which equatorial anomalous westerlies are strongest, roughly over South America, weak anomalous cyclones straddle the equator.

At day −2 (Fig. 5c), the leading edge of the low OLR anomaly is over the continent. The easterlies to the west and westerlies to the east are consistent with the anomalous upper-level divergence one would expect to be collocated with a convective anomaly, but the streamfunction anomalies are still weak. Figure 5d shows the day −1 anomalies: the fields are similar to those on day −2, except that the OLR anomaly is substantially farther to the east. On day 0 (Fig. 5e) the OLR anomaly is located over the base point. The twin anticyclones straddling the equator to the west of the OLR anomaly are the expected response to a heat source over the equator (e.g., Gill 1980). On day 1, the OLR anomalies have progressed farther eastward (not shown).

d. South America precursor

The evolution of the convection–circulation pattern associated with prior OLR anomalies over South America (Fig. 6) is quite different and shows much more structure than the composite based on antecedent eastern Pacific anomalies (Fig. 5). The quantities plotted in Fig. 6 are the same as in Fig. 5, except geopotential height replaces streamfunction. Additionally, Fig. 7 shows 850-mb wind, 850-mb height, and precipitation anomalies, while Fig. 8 shows 1000-mb wind and height anomalies, and total precipitation. All three figures show the same leads.

One striking contrast between the events with Pacific precursors and those with South American precursors is that while the former display only weak anomalies at low levels (which are not shown for that reason), the low-level circulation anomalies for the latter are quite prominent. At day −4, height anomalies are already evident at 200 (Fig. 6a), 850 (Fig. 7a), and 1000 mb (Fig. 8a), part of an arching wave train extending westward from the domain shown to at least the subtropical date line. Over the Pacific, the anomalies tilt slightly westward with height (not shown). Over South America, however, the spatial shift between the 200-mb low, which is centered over central Argentina, and those at lower levels, which are centered over extreme northern Argentina and whose elongation is primarily meridional, is more pronounced. The increase in the vertical tilt and elongation at lower levels as the synoptic low crosses the Andes has been previously observed (e.g., Gan and Rao 1994; Seluchi et al. 1998; Vera et al. 2002).

The present composites are quite similar to the composites of summertime cold-air outbreaks east of the subtropical Andes, or ''South American cold surges,'' discussed by Garreaud and Wallace (1998) and Garreaud (2000). Garreaud and Wallace (1998) composited based on an OLR convective index (W m^{-2}; below 230 W m^{-2}) averaged in the 20°–25°S, 60°–55°W region, while Garreaud (2000) based his composites on large surface pressure increases over an area centered at 25°S, 57.5°W. These cold surges were found to greatly impact the organization of deep convection to the north, ahead of the cold-air intrusion.

The negative height anomaly over the continent at day −4 [which corresponds most closely with the ''day −1''

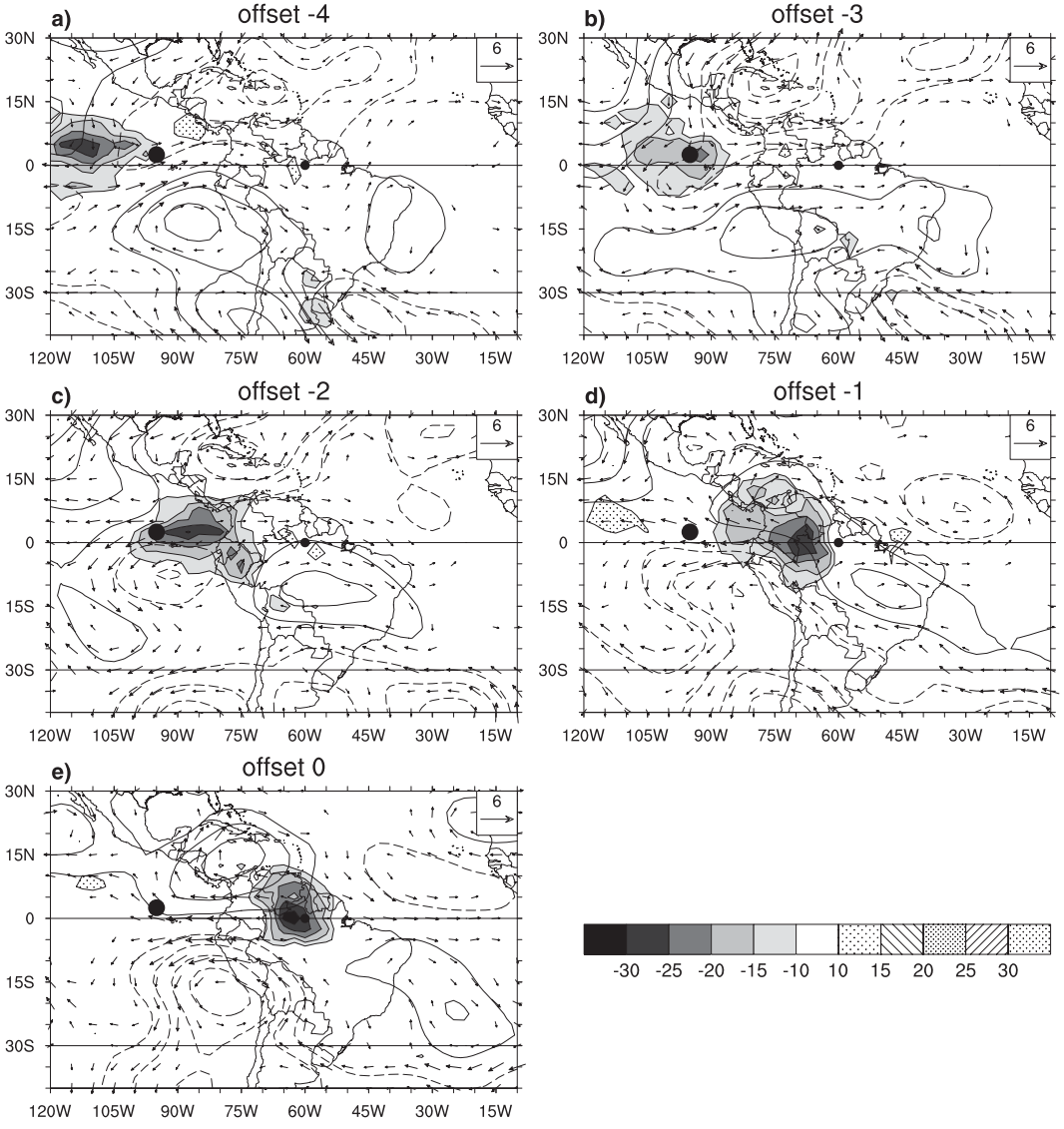

FIG. 5. Composite of 30-day high-pass OLR (shaded) and 200-mb streamfunction (CI = 1×10^6 m^2 s^{-1}) and wind anomalies (vectors). Composites are based on days on which Kelvin-filtered OLR anomalies were at least 1.5 std devs below the mean at 0°, 60°W (small dot over South America), and Kelvin-filtered OLR anomalies 3 days before at 2.5°N, 95°W (large dot over Pacific) were less than -16 W m^{-2} with fields leading the base-point anomaly by the number of days indicated above map. The 0 contour is omitted and negative contours dashed. Reference wind vector (m s^{-1}) is located in upper right.

composite of Garreaud (2000, his Fig. 4d)] is larger at 1000 mb than at 850 mb, implying warm low-level temperatures. This is consistent with an anomalous low-level jet at 850 mb, in approximate geostrophic balance, which brings warm air into the region from the north. At 1000 mb, in contrast, the flow is strongly cross gradient, although Seluchi et al. (2006) showed that surface warming in this type of synoptic situation is due to more subsidence than advection. The positive rainfall anomaly (Fig. 7a) at about 25°S, 60°W is consistent with dynamical forcing by the approaching upper-level trough and is also in the same location as the precipitation associated with a strong South American low-level jet (Liebmann et al. 2004).

The circulation fields at day -3 (Figs. 6b, 7b, and 8b) most closely correspond to the ''day 0'' composite shown in Garreaud (2000). The upper-level wave train has progressed slightly eastward, but strong upper-level geostrophic northwesterly anomalies remain over central South America, near 30°S. The low-level circulation,

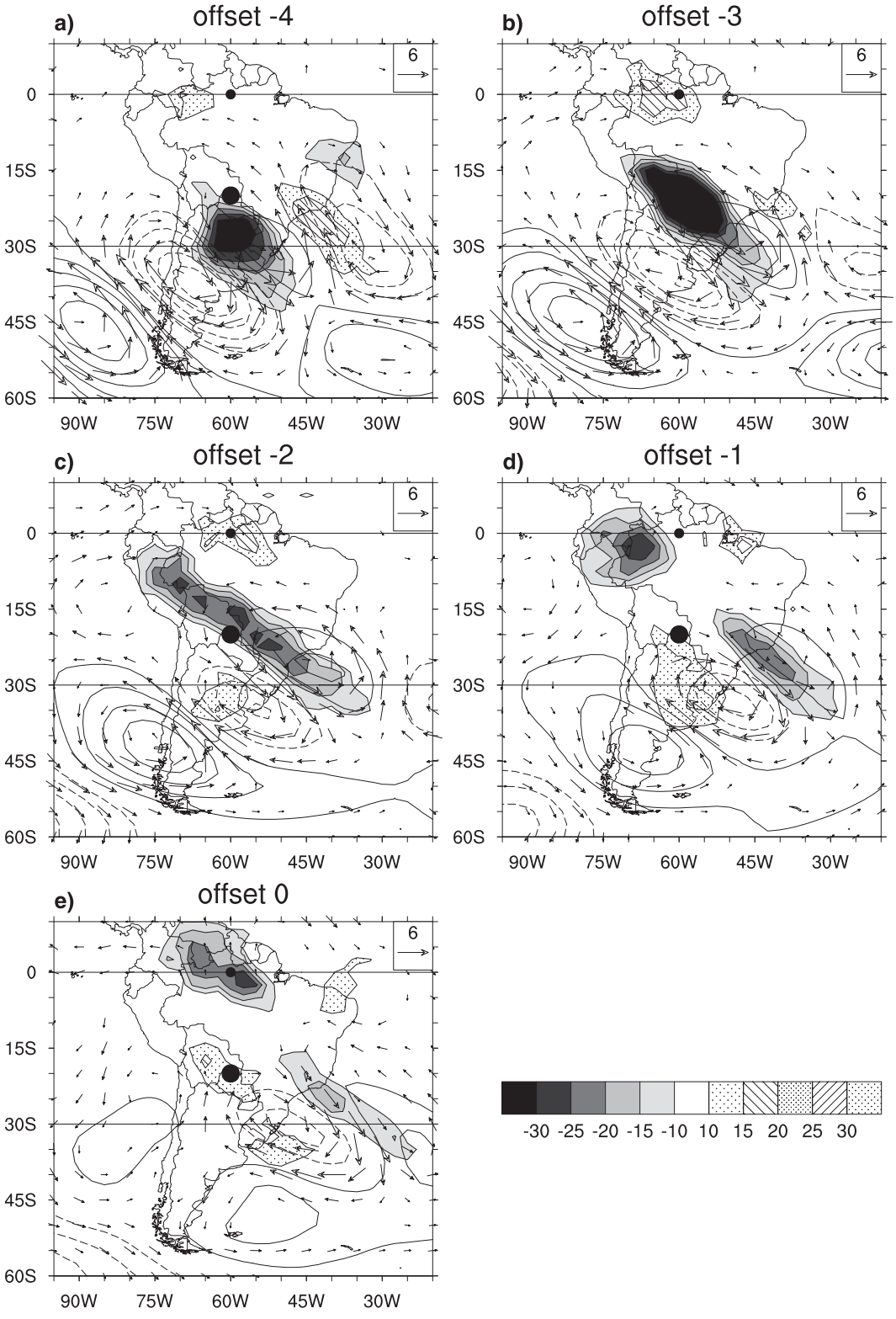

FIG. 6. As in Fig. 5, except the precursor anomaly is lower than 1.5 std devs below mean of 30-day high-pass OLR at 20°S, 60°W (large dot), and contours are of geopotential height anomalies (CI = 10 m, with 0 contour omitted and negative contours dashed). Reference wind vector is 6 m s^{-1}.

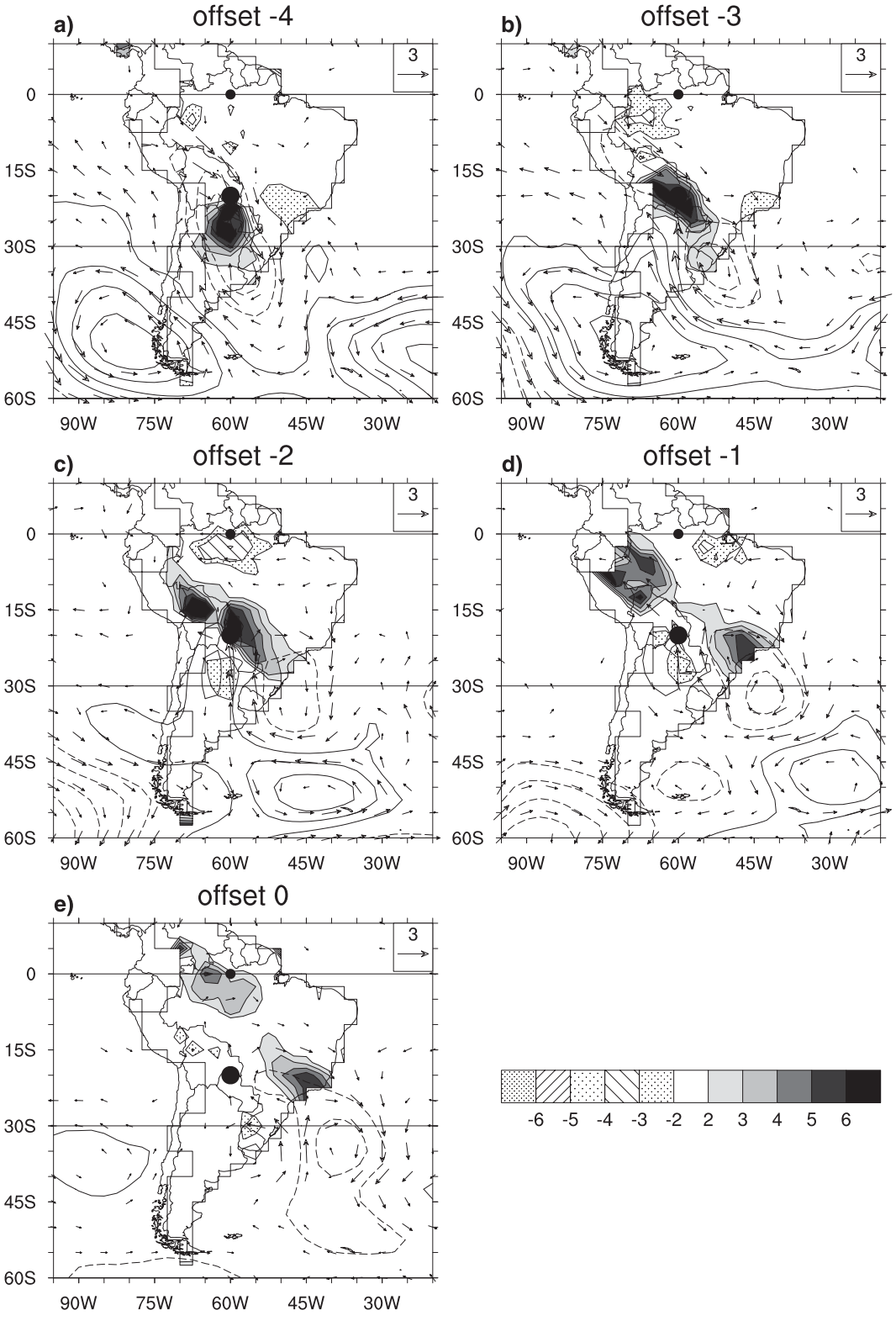

FIG. 7. As in Fig. 6, except height and wind anomalies are at 850 mb (with half the CI and twice the vector length as in Fig. 6) and shaded quantity is high-pass rainfall anomaly (shading, CI: mm day^{-1}). Lines indicate perimeter of rainfall data coverage.

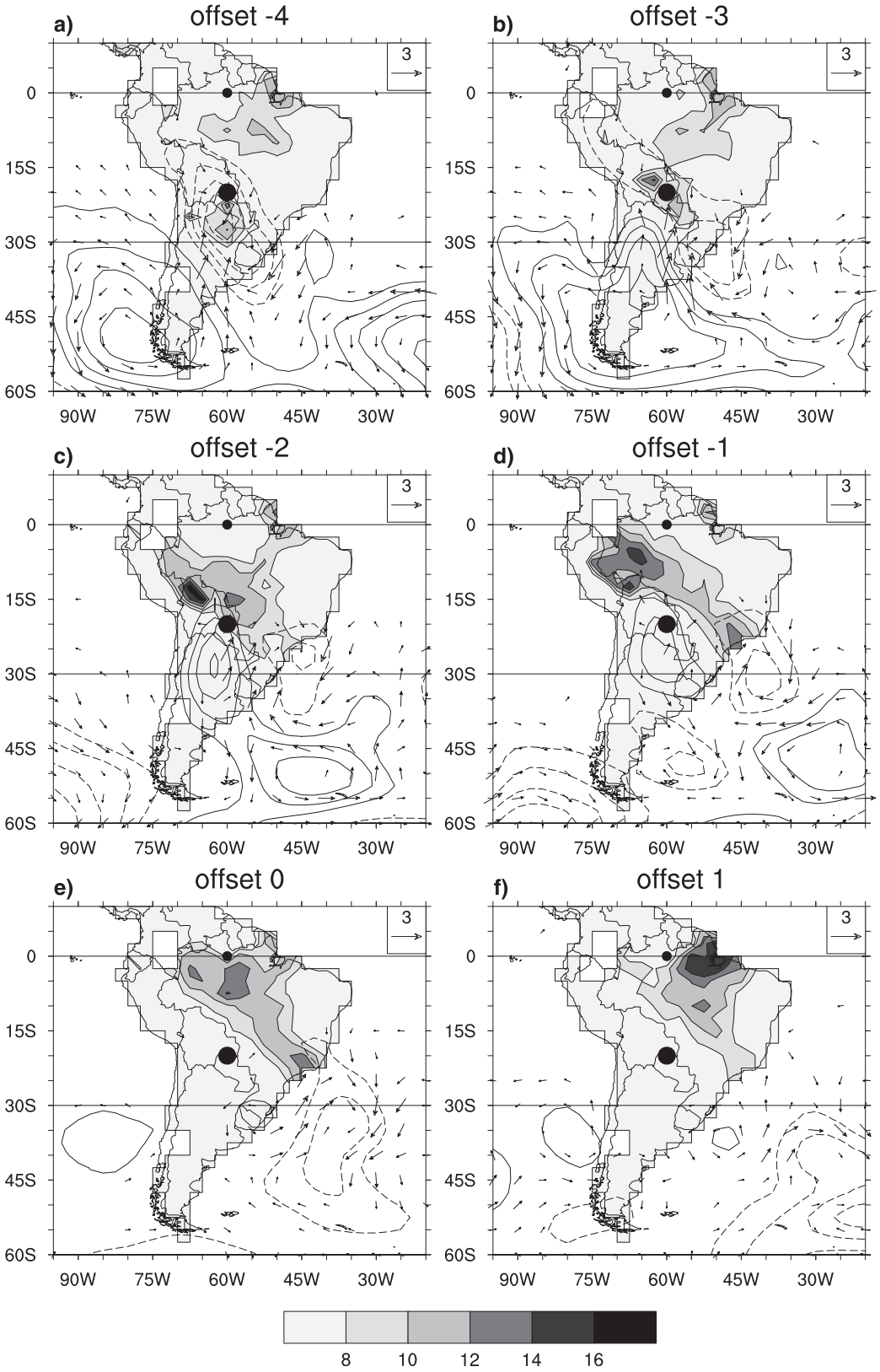

FIG. 8. As in Fig. 7, except height and wind anomalies are at 1000 mb, and shaded quantity is unfiltered rainfall (mm day^{-1}). Day +1 is also included.

however, has changed dramatically. At 850 mb the trough that is evident on the previous day has weakened substantially and retreated southward. A low-level high is beginning to push from the southeastern Pacific into the continent. The development of this high is a consequence of strong anticyclonic vorticity advection at midtropospheric levels on the east side of the Andes (see Marengo et al. 1997; Garreaud 1999, 2000). The strong 850-mb northerly anomalies of day −4 (Fig. 7a) are no longer evident. Instead, there are strong southerlies at about 60°W, behind the trough. There is now a nearly complete reversal of wind anomalies between 200 and 850 mb. Ageostrophic southerlies at 1000 mb, resulting from blocking of the flow by the Andes, advect cold air to the north, which marks the beginning of the cold surge (Garreaud and Wallace 1998). Both negative OLR and positive precipitation anomalies have strengthened and moved northward and, as expected, now align with the secondary base point. Negative precipitation anomalies reside near the equator.

On day −2 (Figs. 6c, 7c, and 8c) rainfall and, especially, OLR anomalies have become elongated, suggestive of a cold front, located slightly southwest of the mean position of the SACZ (e.g., Nogués-Paegle and Mo 1997; Carvalho et al. 2004). Low-level southerly winds behind the front are nearly geostrophic at 850 mb, and are nearly down gradient and perpendicular to the front at 1000 mb. The height anomalies are again stronger at 1000 mb than at 850 mb, indicative of cold air near the surface. Negative precipitation anomalies are found behind the front and at the equatorial base point. Along the front, total rainfall is about 10 mm day^{-1}.

The upper-level wave train has moved slightly northeastward by day −1 (Fig. 6d). Ahead of the anomalous trough, which is now centered slightly off the coast of the continent, negative OLR anomalies and positive precipitation anomalies are found (Figs. 6d and 7d), and the total precipitation map (Fig. 8d) indicates an active SACZ. The interesting aspect of the precipitation pattern, however, is the positive anomaly located over northwestern South America that has become detached from that associated with the upper-level trough (although the raw precipitation still shows it as a continuous band, Fig. 8d). There is little in the upper-level geopotential (or streamfunction) field to suggest forcing of this anomaly, which arrives at the base point the following day. Rather, there are still weak southerly anomalies at lower levels, which continue to advect cold air toward the equator.

On day 0 (Figs. 6e, 7e, and 8e), the circulation anomalies along the equator appear to be rather small and disorganized. In subsequent days (not shown), the OLR anomaly does not continue its northward progression into the Northern Hemisphere, but rather begins to propagate eastward along the equator, apparently as an organized Kelvin wave (see also Fig. 9), potentially reaching the coast of Africa and affecting precipitation in this region (Wang and Fu 2007).

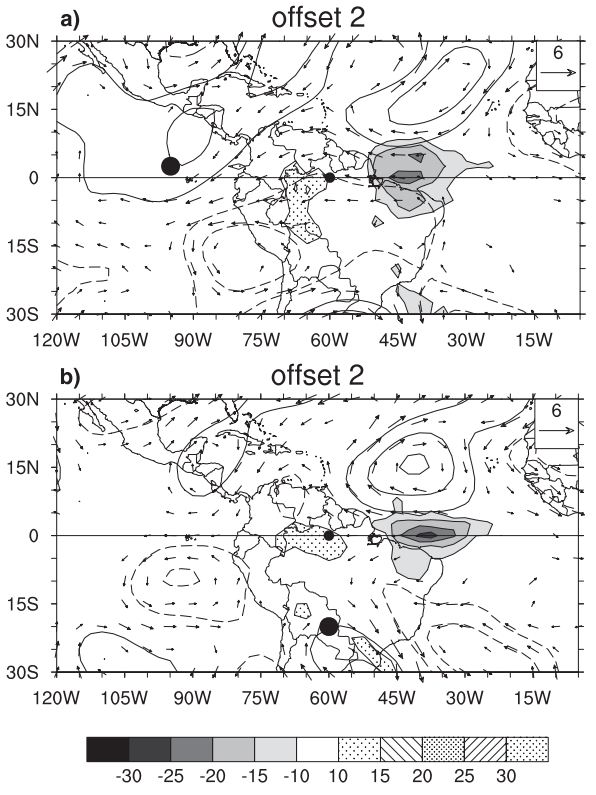

FIG. 9. Composite of dates used for (a) Fig. 5 (Pacific precursors) and (b) Figs. 6, 7, and 8 (South America precursors) for day +2. Composited quantities are high-pass-filtered OLR and 200-mb streamfunction and wind. Shading, vectors, and contours are same as in Fig. 5.

The resemblance between the composites based on antecedent negative OLR anomalies in central South America and the cold-air incursions identified by Garreaud and Wallace (1998) and Garreaud (2000) suggests that some of these incursions may induce near-equatorial convection, ultimately leading to the formation of Kelvin waves. Garreaud (2000), however, noted that in their composites the cold-air incursions vanish as they approach the equator, as a result of strong low-latitude surface heating. Thus, we speculate that only the strongest of these cold-air outbreaks reach the low latitudes before dissipating, so that their remnants may force Kelvin waves at the equator. During winter, strong cold surges are known to reach the equator (e.g., Parmenter 1976).

The precise origin of Kelvin wave signals appears to be unimportant for their evolution following the key date (day 0). Figure 9 shows that the Pacific precursor and the South America precursor composites on day +2 are quite similar, even though they are computed from almost independent dates (only four dates are common). Their similarity continues as the convective anomaly propagates into the Atlantic (not shown). This confirms that Kelvin waves that propagate from South America into the Atlantic can result from more than one mechanism.

e. Other considerations

Of course, the 53 preexisting Kelvin wave events propagating from the eastern Pacific and the 48 Kelvin events that are triggered in situ by the remains of a cold surge over South America are only a small fraction of the 299 independent Kelvin events identified at the base point (which themselves cover only a small fraction of the 27 winters in the record). It is not correct, however, to conclude that 2/3 of all Kelvin events are not associated with either phenomenon. Recall that the criteria chosen for compositing were subjective: if the base-point threshold or the precursor thresholds were set to lower values, more events of each type would be identified, although they would be weaker than those found with the present (conservative) thresholds. On the other hand, substantial variance within the Kelvin wave band is associated with processes other than Kelvin waves. Thus, it is quite difficult to provide an accurate assessment of the ''impact'' of Kelvin waves. One estimate, given above, suggests that about 15% of total variance in OLR can be explained by the Kelvin wave band.

Another measure of the influence of Kelvin waves can be obtained by averaging the rainfall associated with both types of Kelvin events (Pacific and cold-surge events) and comparing it with climatological values. Precipitation at 0°, 60°W increases from a climatological average of 5.6 mm day^{-1} for the November–May season to 8.4 mm day^{-1} at day 0, a 49% increase in the daily rate. At day +1 the daily rate at 2.5°S, 52.5°W, near the mouth of the Amazon River increases by 86%, from 7.6 to 14.1 mm day^{-1}. Northeast Brazil also feels the influence of these disturbances; for example, on day +2 at 5°S, 37.5°W, the average rainfall increases by 43% with respect to climatology, from 3.4 to 4.8 mm day^{-1}. Thus, while these events do not necessarily represent a large fraction of the days of the period under investigation, precipitation does tend to be elevated for a day or more before and after the peak day.

While it is difficult to determine the exact contribution of Kelvin waves to the rainfall climatology, the following two points should be emphasized: one is that Kelvin waves may form over South America with neither a Pacific nor a cold wave precursor; the other is that not all cold surges, even strong ones that reach the equator, result in Kelvin waves.

To demonstrate that Kelvin waves can form without large precursors in either the equatorial Pacific or South America, a procedure similar to that used to isolate Kelvin waves is developed to remove events with precursors. From the original list of 299 Kelvin wave events at 0°, 60°W, events with precursors of at least -8 W m^{-2} of Kelvin-filtered OLR at 2.5°N, 95°W and of 30-day high-pass OLR at 20°S, 60°W are removed, leaving 96 dates (note that the precursor threshold is weaker than that previously used, so that the procedure also removes weak precursor events).

The composite for day -3 (Fig. 10a) contrasts markedly with the corresponding map for events with either Pacific or South American precursors (Figs. 5b and 6b) in that there are no visible negative OLR anomalies in the entire domain. The following day (Fig. 10b), a weak convective anomaly forms on the east slope of the Andes; on day -1 (Fig. 10c) this anomaly has increased and is in about the same location (although slightly weaker) as the anomaly associated with cold surges (Fig. 6d). Also visible in Fig. 10c is a wave train propagating equatorward from the South Pacific, which is weaker and located farther west than that associated with cold surges (Fig. 6). This wave train bears a marked resemblance to the pattern identified as a precursor to west tropical Pacific Kelvin waves by Straub and Kiladis (2003a), where a subtropical anticyclone is located just poleward of the Kelvin OLR anomaly. The OLR anomaly continues to propagate eastward, so that by day +2 (Fig. 10d) it resembles the composites shown in Fig. 9 and therefore is again suggestive of a Kelvin wave.

Other mechanisms by which Kelvin waves appear to form in situ over equatorial South America are not completely apparent from our analyses, although there are multiple possibilities. One possibility is that the composite encompasses many events that are remotely forced, but each event is sufficiently different that the composite is almost featureless until just before the key date. These disturbances can ''project'' onto the Kelvin wave structure, exciting a Kelvin response (e.g., Hoskins and Yang 2000; Straub and Kiladis 2003a).

It is also plausible that the Kelvin events with no apparent precursor form from in situ convection over the east slope of the mountains, owing to orographic uplift from mean easterly low-level winds, and that, once formed, they propagate eastward. Kleeman (1989) discussed yet another possibility, that a transient equatorial heat source will produce a source of Rossby

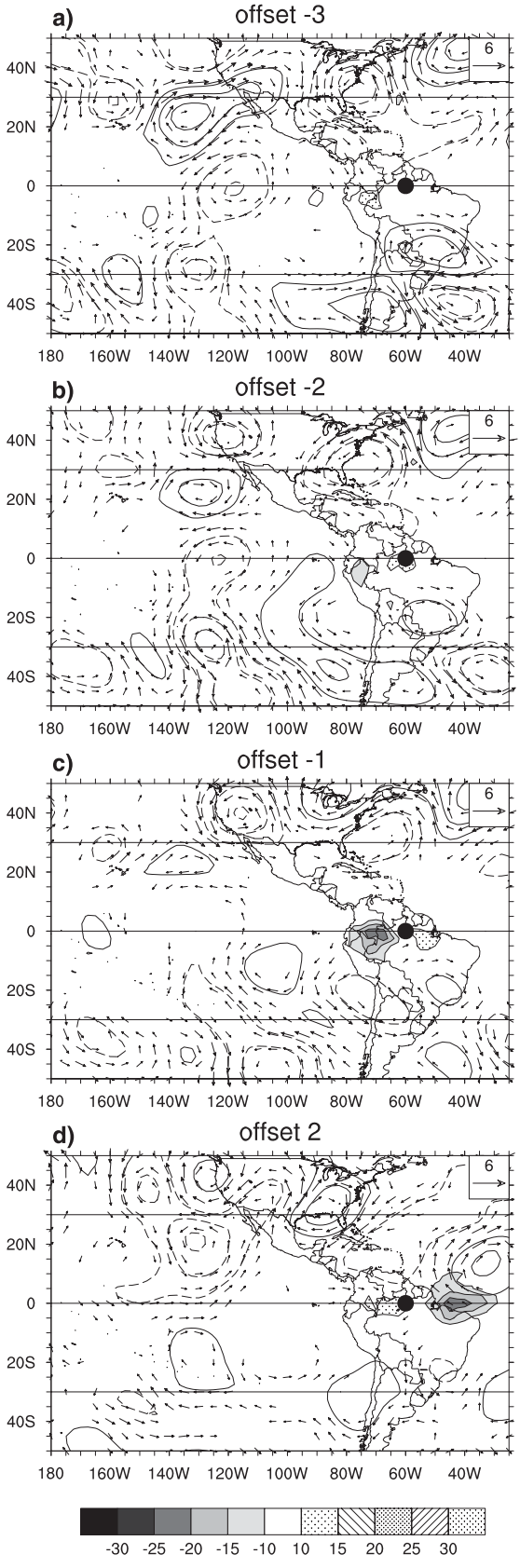

waves, which can then scatter off a boundary to the west and partially reflect as baroclinic Kelvin waves.

To demonstrate that cold surges can cause convection on the equator that does not force a Kelvin wave, the same calculation used to produce the cold-surge composite shown in Figs. 6, 7, and 8 was repeated, except that a threshold of 2 standard deviations of *30-day high-pass-filtered* OLR is used to determine convective anomalies at 0°, 60°W and the precursor anomalies at 20°S, 60°W are required to be at least -24 W m^{-2}. This leaves 58 events, after excluding 6 events that also enter the ''cold surge'' composite shown previously to result in a Kelvin wave. The result is a composite (Fig. 11) that in many ways resembles the composite cold-surge event of Fig. 6, although the OLR anomalies, which depend on the chosen threshold, are somewhat weaker. The subtropical height anomalies, on the other hand, are stronger in some cases and tend to display a more zonal orientation after day -4. Furthermore, although at day -1 (Fig. 11c) there is a substantial OLR anomaly at the equator west of the base point, in the days following the key date (Figs. 11d,e) this OLR disturbance dies out rather rapidly. This is in marked contrast with the anomalies composited from Kelvin-filtered OLR (Fig. 9b), which are still propagating into the Atlantic on day $+2$.

f. Interannual variability

In the Pacific, it is logical to expect that the closer to the coast of South America a Kelvin wave is initiated, the more likely it will be to reach the central continent. It is further expected that convective activity along the equator could excite Kelvin waves in situ, for instance, by the reflection of Rossby wave energy off the eastern side of the Andes (Kleeman 1989). As we have shown above, and as Straub and Kiladis (2003a) also demonstrated, Kelvin waves can also be forced by midlatitude synoptic disturbances, possibly even if such forcing does not propagate far into the tropics (Hoskins and Yang 2000). Therefore, the interannual variability of Kelvin waves may be affected by the presence or absence of convective activity in the central to eastern Pacific, as well as extratropical wave activity. However, because the composites do not show any systematic extratropical signals apart from the cold surges, it is difficult to test the latter hypothesis, although it is more straightforward to test whether the ''supply'' of Kelvin waves from the Pacific affects the activity over South America.

←

FIG. 10. Same as in Fig. 9 except composite of events at 0°, 60°W that are related neither to Pacific precursors nor to South America precursors, for stated leads and lags.

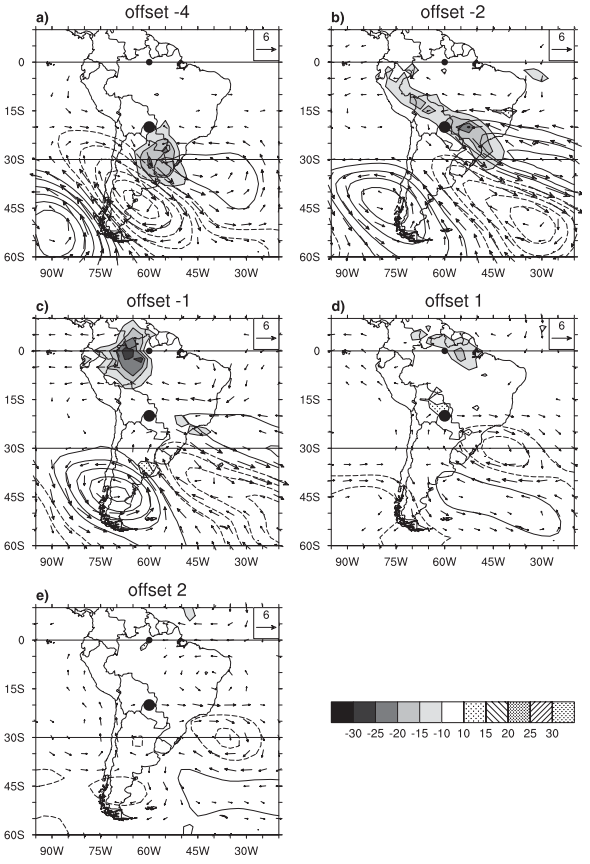

FIG. 11. As in Fig. 6, except that dates are based on 2.0 std dev anomalies of 30-day high-pass OLR anomalies (and a precursor over South America at day −3 of at least 24 W m^{-2}), and those dates in common with the dates composited in Fig. 6 are removed. Lead and lags differ from Fig. 6.

Two phenomena that are known to modulate convective activity in the equatorial Pacific region are El Niño–Southern Oscillation (ENSO) and the Madden–Julian oscillation (MJO; e.g., Madden and Julian 1994). Straub and Kiladis (2003b,c) showed statistically that Pacific Kelvin wave activity is enhanced during El Niño, and also following the arrival of an MJO in the western Pacific warm pool region.

Warm SSTs in the central to eastern Pacific associated with El Niño are closely tied to enhanced convection there. The average SST in the Niño-3.4 area (5°N–5°S, 120°–170°W) is a common index used to measure the state of ENSO and is computed and archived by the Climate Prediction Center at the U.S. National Centers for Environmental Prediction. The events used for the Pacific composites (Fig. 5) are tallied by year, and the result is correlated with the Niño-3.4 index computed for the period from November to May. The correlation between these two time series is 0.59, which statistically significant by any measure, indicating that during seasons when SSTs are warm in the central Pacific there tends to be an increase in the number of Kelvin events over South America with a precursor in the eastern Pacific. Because there are only about two events per year on average, the correlation is again calculated, but this time the number of events is increased by lowering the thresholds so as to include anomalies lower than −1 standard deviation at the base point and lower than −8 W m^{-2} at day −3 in the Pacific. There are now 229 events; the interannual correlation between the count per year and Niño-3.4 SST is 0.47 (still statistically significant).

The correlation between the number of Kelvin events with a South American precursor reminiscent of cold surges and the Niño-3.4 index is weakly negative and not statistically significant. Nevertheless, it is consistent with the results of Müller et al. (2000), who showed that there tends to be more frost events in the ''Pampas'' of central Argentina during La Niña than El Niño events.

The Madden–Julian oscillation is determined to be either active or inactive on a daily basis using a technique developed by Jones (2009). The interannual correlation between the number of Pacific events and the count of days with an active MJO between November and May, however, is quite low. This is also in agreement with the results of Straub and Kiladis (2003b), who showed that although the MJO substantially modulated Kelvin wave activity within the Pacific ITCZ, its impact on South American Kelvin waves was minimal.

4. Summary and conclusions

Kelvin wave activity over South America is strongest from November to May. Two mechanisms for forcing convective anomalies along the equator over South America that subsequently lead to Kelvin wave activity over the Atlantic have been identified. The associated circulation anomalies are separated by requiring precursor anomalies over either the eastern Pacific or central South America. The Pacific cases are associated with an upper-level disturbance that propagates along the equator into the longitudes of South America from the west and appears to be a preexisting Kelvin wave. The anomalies at the lower levels are quite weak, presumably because any low-level disturbance is blocked by the presence of the Andes. There is a positive correlation between November–May SSTs in the Niño-3.4 region and the number of Pacific cases during the same period. This is presumed to result from the closer proximity of South America to the region of Pacific convective activity when warm SSTs are displaced eastward relative to their usual position.

Those cases with precursors over South America resemble the cold surges identified by Garreaud and Wallace (1998) and Garreaud (2000). A synoptic wave train propagates over South America from the South Pacific and sets up a circulation in which low-level southerly winds advect cold air toward the equator, triggering an elongated band of deep convection ahead of the cold air. Subsequently, remnants of this organized convection propagate toward the equator where they set up the conditions for the initiation of a Kelvin wave. Garreaud (2000) noted that by the time most of these cold surges reach the equator they have all but dissipated, owing to surface heating. This result leads us to speculate that the cases identified here correspond to the strongest of the cold surges.

Cases of convective anomalies over equatorial South America with no visible precursors in either the Pacific or South America, but that propagate into the Atlantic as a Kelvin wave, are also identified. It is not clear whether these disturbances actually form in situ, or are aided by a variety of remote mechanisms that are obscured by the composite such as the reflection of Rossby wave energy off the Andes (Kleeman 1989), or other extratropical wave activity over the Pacific (Hoskins and Yang 2000).

There is also some evidence of cold surges forcing convection at the equator that does not result in a Kelvin wave. This evidence comes from a composite based on dates with large 30-day high-pass-filtered anomalies at the base point, from which the dates that coincide with large Kelvin-filtered anomalies were removed. This composite resembles a cold surge similar to that found by compositing about Kelvin-filtered anomalies, although it is somewhat weaker and is associated with more zonally propagating circulation anomalies. Such structural differences, along with the modulation of mesoscale disturbances by Kelvin waves over South America, are the topic of ongoing work.

Acknowledgments. Ileana Bladé acknowledges support from Grant CGL2005-06600-C03-02 from the Spanish Ministry of Science. The authors wish to thank both reviewers for their insightful and useful comments. Figure 1 was computed from data in the CLAUS archive held at the British Atmospheric Data Centre, produced using ISCCP source data distributed by the NASA Langley Data Center. We also wish to acknowledge support from the NOAA CPPA program.

REFERENCES

Carvalho, L. M. V., C. Jones, and B. Liebmann, 2004: The South Atlantic convergence zone: Intensity, form, persistence, and relationships with intraseasonal to interannual activity and extreme rainfall. *J. Climate,* **17,** 88–108.

Duchon, C. E., 1979: Lanczos filter in one and two dimensions. *J. Appl. Meteor.,* **18,** 1016–1022.

Dunkerton, T. J., and F. X. Crum, 1995: Eastward propagating ~2- to 15-day equatorial convection and its relation to the tropical intraseasonal oscillation. *J. Geophys. Res.,* **100,** 25 781–25 790.

Fu, R., B. Zhu, and R. Dickinson, 1999: How do the atmosphere and land surface influence the seasonal changes of convection in tropical Amazon? *J. Climate,* **12,** 1306–1321.

Gan, M. A., and V. B. Rao, 1994: The influence of the Andes Cordillera on transient disturbances. *Mon. Wea. Rev.,* **122,** 1141–1157.

Garreaud, R. D., 1999: Cold air incursions over subtropical and tropical South America: A numerical case study. *Mon. Wea. Rev.,* **127,** 2823–2853.

——, 2000: Cold air incursions over subtropical South America: Mean structure and dynamics. *Mon. Wea. Rev.,* **128,** 2544–2559.

——, 2001: Subtropical cold surges: Regional aspects and global distribution. *Int. J. Climatol.,* **21,** 1181–1197.

——, and J. M. Wallace, 1998: Summertime incursions of midlatitude air into subtropical and tropical South America. *Mon. Wea. Rev.,* **126,** 2713–2733.

Gill, A. E., 1980: Some simple solutions for heat-induced tropical circulation. *Quart. J. Roy. Meteor. Soc.,* **106,** 447–462.

Hodges, K. I., D. W. Chappell, G. J. Robinson, and G. Yang, 2000: An improved algorithm for generating global window brightness temperatures from multiple satellite infrared imagery. *J. Atmos. Oceanic Technol.,* **17,** 1296–1312.

Hoskins, B. J., and G.-Y. Yang, 2000: The equatorial response to higher-latitude forcing. *J. Atmos. Sci.,* **57,** 1197–1213.

Jones, C., 2009: A homogeneous stochastic model of the Madden–Julian oscillation. *J. Climate,* in press.

Kalnay, E., and Coauthors, 1996: The NCEP/NCAR 40-Year Reanalysis Project. *Bull. Amer. Meteor. Soc.,* **77,** 437–471.

Kleeman, R., 1989: A modeling study of the effect of the Andes on the summertime circulation of tropical South America. *J. Atmos. Sci.,* **46,** 3344–3362.

Liebmann, B., and C. A. Smith, 1996: Description of a complete (interpolated) outgoing longwave radiation dataset. *Bull. Amer. Meteor. Soc.,* **77,** 1275–1277.

——, and D. Allured, 2005: Daily precipitation grids for South America. *Bull. Amer. Meteor. Soc.,* **86,** 1567–1570.

——, J. A. Marengo, J. D. Glick, V. E. Kousky, I. C. Wainer, and O. Massambani, 1998: A comparison of rainfall, outgoing longwave radiation, and divergence over the Amazon Basin. *J. Climate,* **11,** 2898–2909.

——, G. N. Kiladis, C. S. Vera, A. C. Saulo, and L. M. V. Carvalho, 2004: Subseasonal variations of rainfall in South America in the vicinity of the low-level jet east of the Andes and comparison to those in the South Atlantic convergence zone. *J. Climate,* **17,** 3829–3842.

Lim, H., and C.-P. Chang, 1983: Dynamics of teleconnections and Walker circulations forced by equatorial heating. *J. Atmos. Sci.,* **40,** 1897–1915.

Madden, R. A., and P. R. Julian, 1994: Observations of the 40–50-day oscillation—A review. *Mon. Wea. Rev.,* **122,** 814–837.

Marengo, J., A. Cornejo, P. Satymurty, C. Nobre, and W. Sea, 1997: Cold surges in tropical and extratropical South America: The strong event in June 1994. *Mon. Wea. Rev.,* **125,** 2759–2786.

Mekonnen, A., C. D. Thorncroft, A. R. Aiyyer, and G. N. Kiladis, 2008: Convectively coupled Kelvin waves over tropical Africa during the boreal summer: Structure and variability. *J. Climate,* **21,** 6649–6667.

Mounier, F., G. N. Kiladis, and S. Janicot, 2007: Analysis of the dominant mode of convectively coupled Kelvin waves in the West African monsoon. *J. Climate,* **20,** 1487–1503.

Müller, G. V., M. N. Nuñez, and M. E. Seluchi, 2000: Relationship between ENSO cycles and frost events within the Pampa Húmeda region. *Int. J. Climatol.,* **20,** 1619–1637.

Nguyen, H., and J. P. Duvel, 2008: Synoptic wave perturbations and convective systems over equatorial Africa. *J. Climate,* **21,** 6372–6388.

Nogués-Paegle, J., and K. C. Mo, 1997: Alternating wet and dry conditions over South America during summer. *Mon. Wea. Rev.,* **125,** 279–291.

Parmenter, F. C., 1976: A Southern Hemisphere cold front passage at the equator. *Bull. Amer. Meteor. Soc.,* **57,** 1435–1440.

Roundy, P. E., 2008: Analysis of convectively coupled Kelvin waves in the Indian Ocean MJO. *J. Atmos. Sci.,* **65,** 1342–1359.

——, and W. M. Frank, 2004: A climatology of waves in the equatorial region. *J. Atmos. Sci.,* **61,** 2105–2132.

Seluchi, M. E., Y. V. Serafini, and H. Le Treut, 1998: The impact of the Andes on transient atmospheric systems: A comparison between observations and GCM results. *Mon. Wea. Rev.,* **126,** 895–912.

——, R. D. Garreaud, F. A. Norte, and A. C. Saulo, 2006: Influence of the subtropical Andes on baroclinic disturbances: A cold front case study. *Mon. Wea. Rev.,* **134,** 3317–3335.

Straub, K. H., and G. N. Kiladis, 2002: Observations of a convectively coupled Kelvin wave in the eastern Pacific ITCZ. *J. Atmos. Sci.,* **59,** 30–53.

——, and ——, 2003a: Extratropical forcing of convectively coupled Kelvin waves during austral winter. *J. Atmos. Sci.,* **60,** 526–543.

——, and ——, 2003b: The observed structure of convectively coupled Kelvin waves: Comparison with simple models of coupled wave instability. *J. Atmos. Sci.,* **60,** 1655–1668.

——, and ——, 2003c: Interactions between the boreal summer intraseasonal oscillation and higher-frequency tropical wave activity. *Mon. Wea. Rev.,* **131,** 945–960.

Takayabu, Y. N., 1994: Large-scale cloud disturbances associated with equatorial waves. Part I: Spectral features of the cloud disturbances. *J. Meteor. Soc. Japan,* **72,** 433–448.

——, and M. Murakami, 1991: The structure of super cloud clusters observed in 1–20 June 1986 and their relationship to easterly waves. *J. Meteor. Soc. Japan,* **69,** 105–125.

Vera, C. S., P. K. Vigliarolo, and E. H. Berbery, 2002: Cold season synoptic-scale waves over subtropical South America. *Mon. Wea. Rev.,* **130,** 684–699.

Wang, H., and R. Fu, 2007: The influence of Amazon rainfall on the Atlantic ITCZ through convectively coupled Kelvin waves. *J. Climate,* **20,** 1188–1201.

Wheeler, M., and G. N. Kiladis, 1999: Convectively coupled equatorial waves: Analysis of clouds and temperature in the wavenumber-frequency domain. *J. Atmos. Sci.,* **56,** 374–399.

——, ——, and P. J. Webster, 2000: Large-scale dynamical fields associated with convectively-coupled equatorial waves. *J. Atmos. Sci.,* **57,** 613–640.